

# Calculation of the Valence Band Structure in Strained $\text{In}_{0.7}\text{Ga}_{0.3}\text{As}$ Devices with Different Surface Orientation

Pengying Chang<sup>1, 2</sup>, Lang Zeng<sup>2\*</sup>, Xiaoyan Liu<sup>2\*</sup>, Kangliang Wei<sup>2</sup>, Jieyu Qin<sup>1, 2</sup>, Kai Zhao<sup>2</sup>, Gang Du<sup>2</sup>, Xing Zhang<sup>2</sup>  
<sup>1</sup>School of Electronic and Computer Engineering, Peking University, Shenzhen, 518055, China  
<sup>2</sup>Key Laboratory of Microelectronic Devices and Circuits (MOE), Institute of Microelectronics, Peking University, Beijing, 100871, China  
 E-mail: zenglang@ime.pku.edu.cn, xyliu@ime.pku.edu.cn

**Abstract**—Using the eight-band  $k\cdot p$  Hamiltonian approach, the valence band structure of strained  $\text{In}_{0.7}\text{Ga}_{0.3}\text{As}$  is calculated for (001), (110) and (111) orientation. The impact of biaxial strain and uniaxial strain on energy band splitting and warping is investigated. The dependency of the valence band structure on the surface electric field and body thickness is also studied in this work.

**Keywords**—eight-band  $k\cdot p$  method;  $\text{In}_{0.7}\text{Ga}_{0.3}\text{As}$ ; biaxial strain; uniaxial strain; body thickness

## I. INTRODUCTION

III-V compound semiconductors are promising candidates for replacing Si channels beyond the 16-nm node due to its high electron mobility [1]. Recently, high Indium  $\text{In}_{1-x}\text{Ga}_x\text{As}$  has received a lot of attention. Especially,  $\text{In}_{0.7}\text{Ga}_{0.3}\text{As}$  planar thin body MOSFETs, FinFETs or tri-gate, gate-all-around nanowire MOSFETs and Tunneling FETs have been demonstrated experimentally and exhibited outstanding performance for electron transport [2-5] However, the hole mobility in III-V materials tends to be inferior to strained Si. The large gap between electron and hole mobility for III-V semiconductor becomes an important issue for CMOS application. This necessitates the application of performance boosters such as strain engineer to enhance the hole mobility [6-8]. Furthermore, it is meaningful to select and orient the band structure to yield better properties. Hence in this work, the impact of electric field and body thickness on the valence band structure in  $\text{In}_{0.7}\text{Ga}_{0.3}\text{As}$  devices with (001), (110) and (111) orientation is evaluated. We also study strain effects, including both biaxial strain and uniaxial strain, on valence band structure of  $\text{In}_{0.7}\text{Ga}_{0.3}\text{As}$  devices. The results can be helpful to optimize the design of  $\text{In}_{0.7}\text{Ga}_{0.3}\text{As}$  based devices.

## II. SIMULATION METHOD

The valence band structure of strained semiconductor devices under electric field can be calculated by the  $8\times 8$   $k\cdot p$  Hamiltonian approach [9], employing a triangular well approximation and assuming an infinite barrier height at both side of the  $\text{In}_{0.7}\text{Ga}_{0.3}\text{As}$ . Considering the quantum confinement,

This work was supported by the National Fundamental Basic Research Program of China (Grant No. 2011CBA00604) and the National Natural Science Foundation of China (Grant No. 60925015)

$k_z$  is transformed to  $-i\partial/\partial z$  and coordinate  $z$  is perpendicular to the interface. The discretization process of eight-band Hamiltonian is obtained by finite difference method [10]. The space of the in-plane vectors  $\mathbf{K}$  is discretized by building a mesh in polar coordinates. For calculation of the density of states (DOS), the equi-energy lines corresponding to a given energy are calculated. This can be accomplished by inverting the  $k\cdot p$  model in order to obtain an eigenvalue problem for the wave-vector  $\mathbf{K}$  of rank twice as large as the rank of the original problem. When dealing with different crystal orientation, appropriate rotations of the  $k$  space are performed. We take [110] as the channel direction since this is common in PMOS technology. For strained  $\text{In}_{0.7}\text{Ga}_{0.3}\text{As}$ , we consider two cases of technological interest, namely 1) a device under biaxial strain (global strain) due to lattice mismatch and 2) a device stressed by source and drain stressors, inducing uniaxial stress along the channel direction.

Band parameters and deformation potentials for GaAs and InAs are taken from Ref. [11]. All the parameters for  $\text{In}_{0.7}\text{Ga}_{0.3}\text{As}$  are taken as linear interpolation of those of GaAs and InAs except that for the strained energy gap as following [12]:

$$E_g(\text{In}_{1-x}\text{Ga}_x\text{As})=0.324+0.7x+0.4x^2+(a_c-a_v)(\epsilon_{xx}+\epsilon_{yy}+\epsilon_{zz}).$$

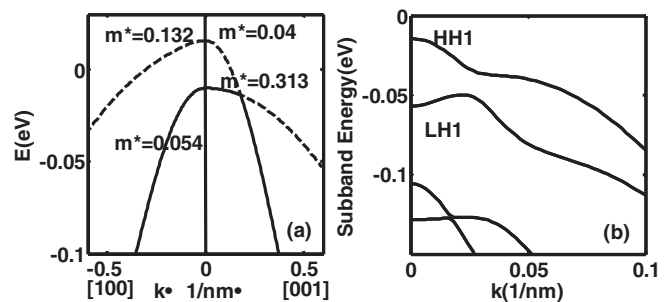


Fig.1 (a) The valence band structure for a bulk  $\text{In}_{0.52}\text{Ga}_{0.48}\text{As}$  (biaxial tension) on InP. (b) The valence subband structure for a 9.4 nm thick  $\text{In}_{0.53}\text{Ga}_{0.47}\text{As}$  (lattice matched).

Fig.1 (a) shows the valence band structure for a bulk  $\text{In}_{0.48}\text{Ga}_{0.53}\text{As}$  (biaxial tension) on InP substrate, and Fig.1 (b) is for a 9.4nm relaxed  $\text{In}_{0.53}\text{Ga}_{0.47}\text{As}$ . The valence band structure and hole effective mass are consistent with the results from Ref [12-13], which verify our simulation method.

### III. RESULTS AND DISCUSSION

#### A. Orientation Dependency

Fig.2 (a-c) illustrate the valence subband structure of a 5nm-thick  $\text{In}_{0.7}\text{Ga}_{0.3}\text{As}$  with (001), (110) and (111) orientation. Fig.2 (d-f) present the energy contours in  $k_x$ - $k_y$  plane for the top two subband ( $n=1, 2$ ) with corresponding orientation. The strong non-parabolic in-plane energy dispersion is shown for the topmost subband with three orientations. It is clearly seen

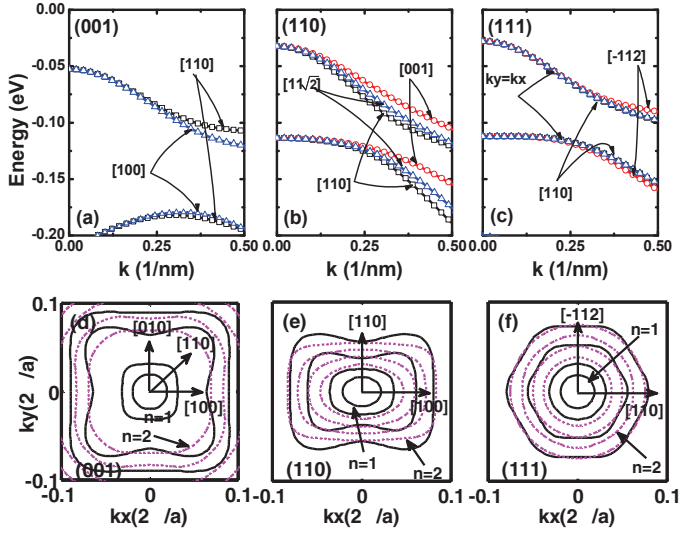


Fig.2 Valence subband structure of a 5nm thick  $\text{In}_{0.7}\text{Ga}_{0.3}\text{As}$  plotted for (001), (110) and (111) surface orientation (a-c). Equi-energy contours of top two subbands ( $n=1,2$ ) are plotted for corresponding orientation. The energies are plotted for 25, 50, 75, 100meV below band-edge  $E(0)$ .

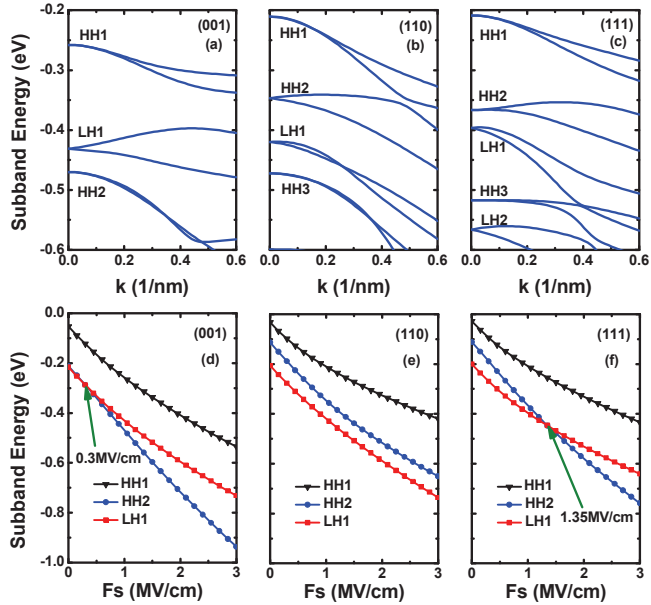


Fig.3 Valence band structures for 5 nm thick  $\text{In}_{0.7}\text{Ga}_{0.3}\text{As}$  under surface electric field  $F_s=1\text{MV/cm}$  [(a)-(c)]. The subband energy shifts at  $\Gamma$  point of top three subband versus electric field  $F_s$  with (001), (110) and (111) orientations are plotted in [(d)-(f)].

that (110) orientation has a lower symmetry than (001) and (111) orientation, and the top two subbands maintain their strong anisotropy.

Fig.3 [(a)-(c)] shows the valence subband structure for  $\text{In}_{0.7}\text{Ga}_{0.3}\text{As}$  under surface electric field  $F_s$  of  $1\text{MV/cm}$  with (001), (110) and (111) orientations. For ground-state subband ( $n=1$ ) energy at  $\Gamma$  point ( $k=0$ ), it is observed that  $E_0(111) \sim E_0(110) > E_0(001)$ . The surface electric field breaks the inversion symmetry of the zinc-blend crystal and leads to a spin split [14]. In Fig.3 [(d)-(f)], the topmost subband shift at  $\Gamma$  point versus  $F_s$  are plotted for different orientation. With the increase of  $F_s$ , there is a crossing point where HH2 and LH1 change position for (001) and (111) orientations. The subband energy shift trend with surface electric field is (001) $>$ (110)  $\sim$  (111).

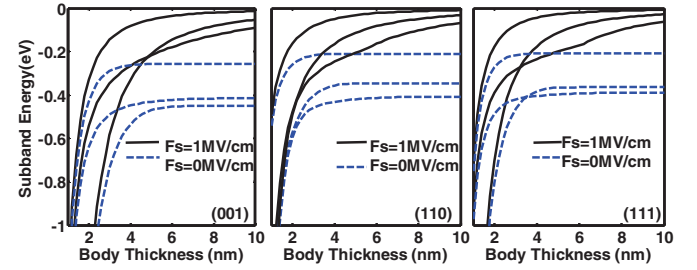


Fig.4 Top three valence subband energies at  $\Gamma$  point versus body thickness, plotted for  $\text{In}_{0.7}\text{Ga}_{0.3}\text{As}$  with (001), (110) and (111) orientation. Surface electric field  $F_s$  of  $1\text{MV/cm}$  (black solid lines) and  $0\text{MV/cm}$  (blue dashed lines) are compared. There is a crossing of the HH2 and LH1 for all orientations as  $T_{\text{body}}$  is decreased.

In Fig.4, the topmost three subband energies at  $\Gamma$  point versus body thickness are presented for  $\text{In}_{0.7}\text{Ga}_{0.3}\text{As}$  devices with  $F_s$  of  $0\text{MV/cm}$  and  $1\text{MV/cm}$ . Under electric field of  $1\text{MV/cm}$ , the subband energies are less sensitive to the decrease of body thickness until the critical thickness, where the size quantization is taking effect. The quantization effect is strongest for (001) orientations, followed by (111) and (110) orientations. This can be explained by the effective quantization mass ( $m_z^*$ ) for the ground state subband, as shown in Fig.5. With the decrease of body thickness,  $m_z^*$  is increasing for (110) orientation.

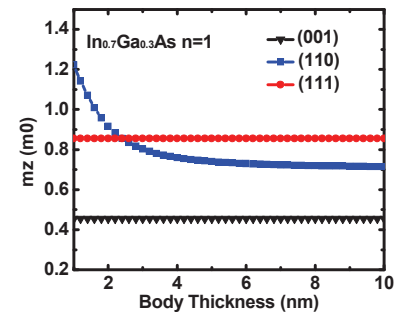


Fig.5 Effective quantization mass  $m_z^*$  for  $\text{In}_{0.7}\text{Ga}_{0.3}\text{As}$ , which is calculated by fitting energy at  $\Gamma$  point to the analytical expression:  $E_0 = (\hbar^2 / 2m_z^*)(\pi / T_{\text{body}})^2$ .

## B. Strain Effect

Fig 6 (a)-(e) show the valence subband structures for unstressed and 1GPa tensile/compressive stressed  $\text{In}_{0.7}\text{Ga}_{0.3}\text{As}$  with electric field  $F_S$  of 1MV/cm respectively. The band structures are plotted along the [110] direction. Strain shifts and warps the valence subband structure. For both biaxial and uniaxial strain, compressive strain pushes the subband upward and warps the band sharply which is beneficial to reduce the

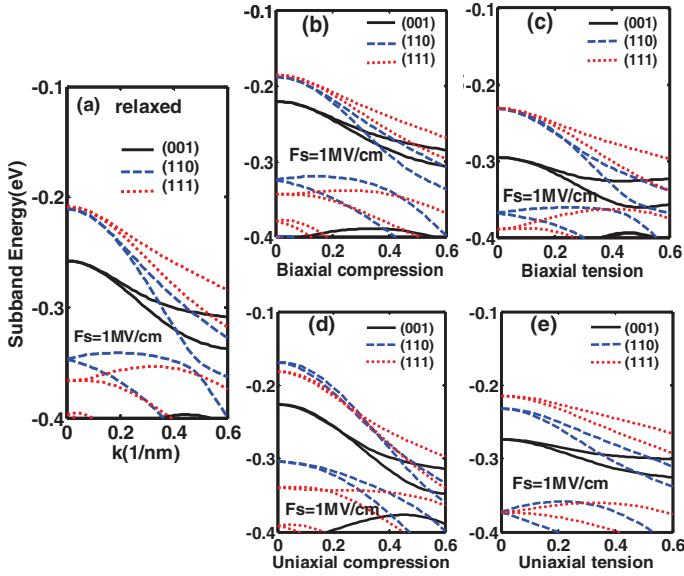


Fig.6 Valence subband energy dispersion along [110] direction in  $\text{In}_{0.7}\text{Ga}_{0.3}\text{As}$  are calculated for (a) relaxed, (b) in-plane biaxial compression, (c) in-plane biaxial tension, (d) [110] uniaxial compression and (e) [110] uniaxial tension with 1GPa external stress. The energies are plotted with (001), (110) and (111) orientation under surface electric field of 1MV/cm.

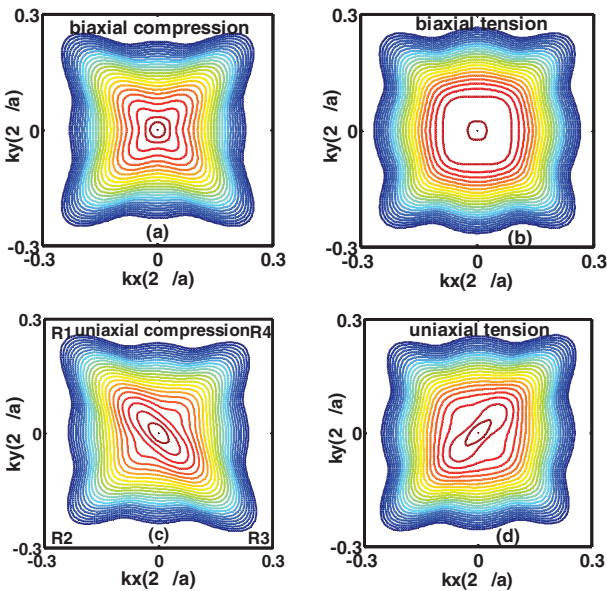


Fig. 7 Equienergy contours are plotted for (001) oriented  $\text{In}_{0.7}\text{Ga}_{0.3}\text{As}$  with  $F_S$  of 1MV/cm under (a) in-plane biaxial compression, (b) in-plane biaxial tension, (c) [110] uniaxial compression and (d) [110] uniaxial tension corresponding to 1GPa stress. The energies are plotted from 25 to 600meV below band-edge  $E(0)$ .

hole effective mass and improve hole mobility. Under tensile strain condition, the subbands are shifted downward and become more flat. For biaxial strain, Energy shift and subband warping is strongest for (001) orientation, followed by (111) and (001) orientation. While for uniaxial strain, the trend is  $(110) > (001) > (111)$ .

Besides, as is illustrated in Fig. 6 (b) and (d), the uniaxial strain induces larger energy shift and more sharp band warping than biaxial strain. To explain this, equi-energy contours are plotted for stressed (001) oriented  $\text{In}_{0.7}\text{Ga}_{0.3}\text{As}$  with  $F_S=1\text{MV/cm}$  in Fig. 7 (a)-(d). Comparing to biaxial strain, the presence of shear component for uniaxial strain contributes to different band warping and results in an in-plane repopulation of the carriers. Uniaxial compression leads to a carrier repopulation from high transport  $m_h^*$  regions R2, R4 to low transport  $m_h^*$  regions R1, R3.

Fig. 8 shows the density of states (DOS) for (001) oriented  $\text{In}_{0.7}\text{Ga}_{0.3}\text{As}$ . Fig. 8 (a) and (b) are plotted for relaxed  $\text{In}_{0.7}\text{Ga}_{0.3}\text{As}$  with  $F_S=0\text{MV/cm}$  and  $F_S=1\text{MV/cm}$ , and the surface electric field reduces the DOS. Under compressive strain (Fig.8 (c) and (e)), DOS decreases. On the contrary, compressive strain (Fig.8 (d) and (f)) increases the DOS.

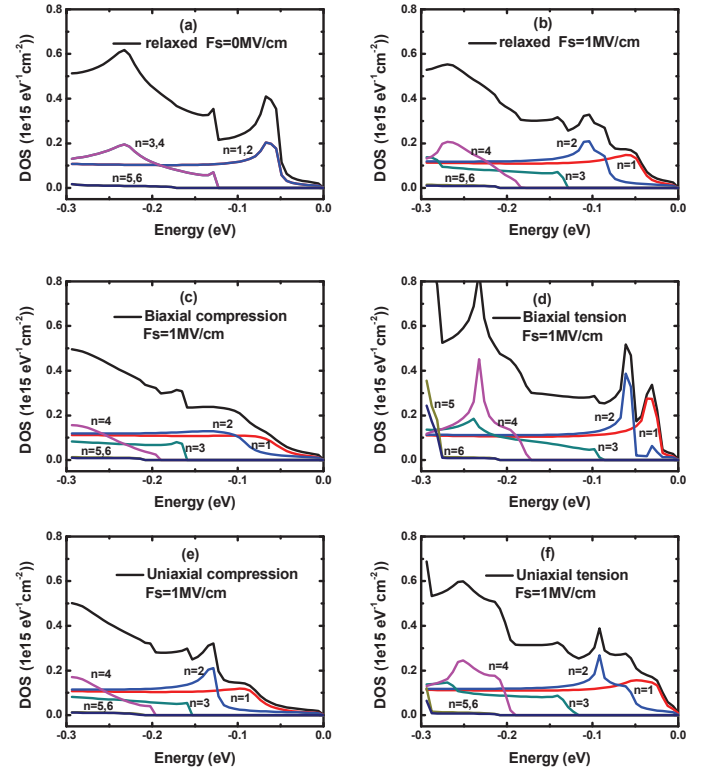


Fig.8 The density of states versus the energy (referred to the ground-state subband at  $k=0$  point) for valence subband of relaxed and stressed  $\text{In}_{0.7}\text{Ga}_{0.3}\text{As}$  for (001) orientation. The subband and total DOS are plotted. For black solid lines, contributions from all the subbands are summed.

Fig.9 (a) and (b) show the top three valence subband energies at  $\Gamma$  point versus biaxial and uniaxial stress for (001) oriented  $\text{In}_{0.7}\text{Ga}_{0.3}\text{As}$  with electric field  $F_S$  of 0MV/cm and

1MV/cm. In biaxial tension case, there are two critical stresses. At first critical stress, the position between the HH2 and LH1 is changed. Beyond the second critical stress, LH1 becomes the ground-state. According to our calculation, strain effects on (110) and (110) orientations have the similar tendency of energy shift as (001) orientation. The critical stress for different orientation is exhibited in TABLE I.

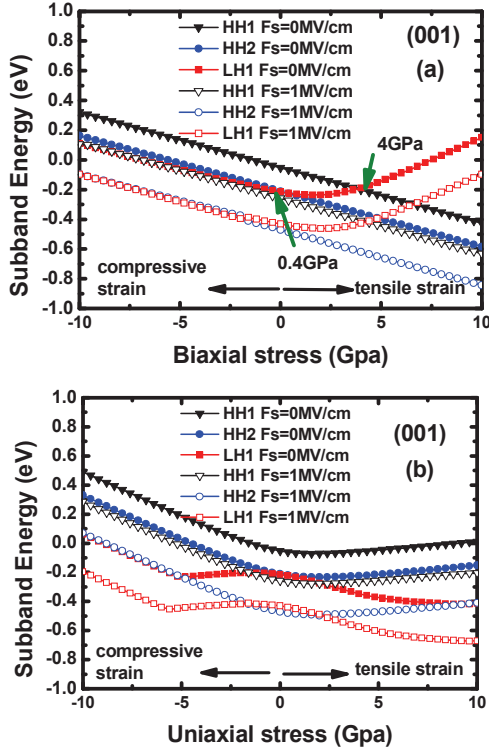


Fig.9 The topmost valence subband energy shift at  $k=0$  point versus external stress for (001) oriented  $\text{In}_{0.7}\text{Ga}_{0.3}\text{As}$  with biaxial (a) and uniaxial (b) strain. Surface electric field  $F_s$  of 0MV/cm and 1MV/cm are compared.

**TABLE I** CRITICAL STRESS FOR SUBBAND CROSSING UNDER BIAxIAL TENSION CASE

Orientation	(001)	(110)	(111)
1 <sup>st</sup> crossing(GPa)	0.4	5.2	4.4
2 <sup>nd</sup> crossing(GPa)	3.6	6	6.4

#### IV. CONCLUSION

The dependency of the valence subband structure on orientation, surface electric field and body thickness in  $\text{In}_{0.7}\text{Ga}_{0.3}\text{As}$  devices is presented. Electric field and body thickness have smallest impact on (110) orientation, due to its large effective quantization mass  $m_z^*$ , followed by (111) and (001) orientations. For the biaxial strain, the strain effects on

the modulation of the band structure: (001) $\rightarrow$ (110) $\sim$ (111) orientation. While for the uniaxial strain: (110) $\rightarrow$ (001) $\rightarrow$ (111) orientation, resulting from the smallest transport  $m_h$  along [110] direction for (110) orientation. Both biaxial and uniaxial compressive strain is beneficial to reduce the hole effective mass and may be advantageous to improve the hole mobility. Especially, the uniaxial compression leads to not only more band warping than biaxial strain but a carrier repopulation from high transport effective mass region to low transport effective mass region.

#### REFERENCES

- [1] Jesus A. del Alamo, "Nanometre-scale electronics with III-V compound semiconductors," *Nature*, vol. 479, pp. 317-323, November 2011.
- [2] G. Dewey, B. Chu-Kung, R. Kotlyar, M. Metz, N. Mukherjee, and M. Radosavljevic, "III-V Field Effect Transistors for Future Ultra-Low Power Applications," *VLSI Tech. Dig.*, pp. 45-46, 2012.
- [3] J. J. Gu, Y. Q. Liu, Y. Q. Wu, R. Colby, R. C. Gordon, and P. D. Ye, "First Experimental Demonstration of Gate-all-around III-V MOSFETs by Top-down Approach," *IEDM Tech. Dig.*, pp. 769-772, 2011.
- [4] J. J. Gu, X. W. Wang, J. Shao, A. T. Neal, M. J. Manfra, R. G. Gordon, and P. D. Ye, "III-V Gate-all-around Nanowire MOSFET Process Technology: From 3D to 4D," *IEDM Tech. Dig.*, pp. 529-532, 2012.
- [5] D. K. Mohata, R. Bijesh, Y. Zhu, M. K. Hudait, R. Southwich, Z. Chbili, D. Gundlach, J. Suehle, et. Al., "Demonstration of Improved Heteroepitaxy, Stack and Reduced Interface States Enabling Heterojunction Tunnel FETs with High Drive Current and High On-Off Ratio," *VLSI Tech. Dig.*, pp. 53-54, 2012.
- [6] S. Suthram, Y. Sun, P. Majhi, I. Ok, H. Kim, H. R. Harris, et al., "Strain Additivity in III-V Channels for CMOSFETs beyond 22nm Technology Node," *VLSI Tech. Dig.*, pp 182-183, 2008.
- [7] Aneesh Nainani, Jung Yum, Joel Barnett, Richard Hill, Niti Goel, Jeff Huang, Prashant Majhi, Raj Jammy, and Krishna C. Saraswat, "Study of Piezoresistance under uniaxial stress for technologically relevant III-V semiconductors using wafer bending experiments," *APL*, pp 242110-1, 2010
- [8] Hock-Chun Chin, Xiao Gong, Xinke Liu, Zhe Lin, and Yee-Chia Yeo, "Strained  $\text{In}_{0.53}\text{Ga}_{0.47}\text{As}$  n-MOSFETs: Performance Boost with in-situ Doped Lattice-Mismatched Source/Drain Stressors and Interface Engineering," *VLSI Tech. Dig.*, pp. 244-245, 2009.
- [9] Tomas B. Bahder, "Eight-band k.p model of strained zinc-blende crystals," *PRB*, pp 11 992-12 000, Vol.41, No 17, June 1990.
- [10] M. V. Fischetti, "Six-band k.p calculation of the hole mobility in silicon inversion layers: Dependence on surface orientation, stain, and silicon thickness," *JAP*, pp 1097-1095, Vol.94, No.2, July 2003.
- [11] I. Vurgaftman and J. R. Meyer, "Band parameters for III-V compound semiconductors and their alloys," *JAP*, Vol.89, No.11, June 2001.
- [12] Calvin Yi-Ping and Shun Lien Chuang, "Spin-orbit-coupling effects on the valence-band structure of strained semiconductor quantum wells," *PRB*, Vol.46, No.7, pp 4110-4122, August 1992
- [13] Masaaki Nido et al, "Analysis of Differential Gain in InGaAs-InGaAsP Compressive and Tensile Strained Quantum-Well Lasers and Its Application for Estimation of High-Speed Modulation Limit," *Journal of quantum electronics*, Vol.29, No.3, pp 885-895, March 1993.
- [14] Bradley A. Foreman, "Effective-mass Hamiltonian and boundary conditions for the valence bands of semiconductor microstructures," *PRB*, Vol.48:4964-4967, August 1993